Forward and inverse kinetic energy cascades in Jupiter's turbulent weather layer

Roland M. B. Young & Peter L. Read

Atmospheric, Oceanic and Planetary Physics, Department of Physics,
University of Oxford, UK

Supplementary Information

Contents

1 Estimate of deformation radius

Showman et al. [1] define the Rossby deformation radius as $L_D = NH/f$, where N is the Brunt-Väisälä (buoyancy) frequency $N = \sqrt{g\,\partial \ln\theta/\partial z}$, H is the pressure scale height, and $f = 2\Omega\cos\phi$ is the Coriolis parameter. θ is potential temperature, z is vertical position, Ω is the rotation rate of the planet, ϕ is latitude, and g is gravity.

Following their method and assuming an isothermal, hydrostatic atmosphere with equilibrium temperature T_e, the hydrostatic equation gives a pressure scale height $H = R_d T_e/g$, where R_d is the specific gas constant. Relating potential to absolute temperature in an isothermal atmosphere we get

$$\frac{\partial \ln\theta}{\partial z} = -\frac{\kappa}{p}\frac{\partial p}{\partial z}$$

where $\kappa = R_d/c_p$, and c_p is the specific heat capacity. Using the hydrostatic equation and the ideal gas law we obtain the buoyancy frequency $N = g/\sqrt{T_e c_p}$, and combining with the scale height we get the deformation radius

$$L_D = \frac{R_d}{2\Omega\sin\phi}\sqrt{\frac{T_e}{c_p}}$$

By a simple energy balance we have $T_e = (S(1-A)/4\sigma)^{1/4}$, where S is the solar constant at Jupiter, A is the (bond) albedo, and σ is the Stefan-Boltzmann constant. Hence as a function of latitude the deformation radius is

$$L_D = \frac{R_d}{2\Omega\sqrt{c_p}}\left[\frac{S(1-A)}{4\sigma}\right]^{1/8}\frac{1}{\sin\phi}$$

Putting in the numbers, $R_d = 3750\,\mathrm{J\,K^{-1}\,kg^{-1}}$, $c_p = 12\,360\,\mathrm{J\,K^{-1}\,kg^{-1}}$ [2], $S = 50.66\,\mathrm{W\,m^{-2}}$, $A = 0.343$ [3], $\Omega = 1.758\,65\times10^{-4}\,\mathrm{rad\,s^{-1}}$ [4], and $\sigma = 5.670\,373\times10^{-8}\,\mathrm{W\,m^{-2}\,K^{-4}}$, gives

$$L_D \approx \frac{1000\,\mathrm{km}}{\sin\phi} \tag{S1}$$

Using latitudes from $\phi = 20-40°$, we get $L_D = 1600-2900\,\mathrm{km}$. For a typical midlatitude $\phi = 30°$ we have $L_D \approx 2000\,\mathrm{km}$. This agrees reasonably well with other estimates, e.g. Read et al. [5] (1200–2300 km over $\phi = 20-40°$) and Achterberg & Ingersoll [6] (200–1500 km at $\phi = 30°$, depending on atmospheric composition).

2 Expected form of the second order structure function for a Jupiter-like kinetic energy spectrum

We can relate the kinetic energy spectrum for a 2D turbulent flow to the second order structure function $\langle \delta u_L^2 \rangle = \langle \delta u_L^2 \rangle(r)$ using some results from Davidson [7]. For homogeneous, isotropic turbulence the 1D energy spectrum ($E_1(k)$ in his notation) and the autocorrelation function $\langle \mathbf{u} \cdot \mathbf{u}' \rangle = \langle \mathbf{u} \cdot \mathbf{u}' \rangle(r)$, where $\mathbf{u} = \mathbf{u}(\mathbf{x})$, $\mathbf{u}' = \mathbf{u}(\mathbf{x} + \mathbf{r})$, and $r = |\mathbf{r}|$, are related by the following transform pair [7, equation (8.37)]:

$$E_1(k) = \frac{1}{\pi} \int_0^\infty \langle \mathbf{u} \cdot \mathbf{u}' \rangle \cos(kr)\, dr \qquad \langle \mathbf{u} \cdot \mathbf{u}' \rangle = 2 \int_0^\infty E_1(k) \cos(kr) dk \tag{S2}$$

This transform is the same for 2D and 3D turbulence [P. Davidson, personal communication]. Next we consider the diagonal elements of the second-order velocity correlation tensor in 2D turbulence [7, after equation (10.27)]:

$$Q_{ii} = \langle \mathbf{u} \cdot \mathbf{u}' \rangle = \frac{u^2}{r} \frac{\partial}{\partial r}(r^2 f) \tag{S3}$$

where $f = f(r)$ is the longitudinal velocity correlation function [7, equation (3.13)]. In 2D turbulence [7, p. 565]

$$u^2 = \langle u_x^2 \rangle = \langle u_y^2 \rangle = \frac{1}{2} \langle \mathbf{u} \cdot \mathbf{u} \rangle \tag{S4}$$

and this is a constant. Add and subtract $2u^2$ from equation (S3) and rewrite in differential form:

$$\begin{aligned} \langle \mathbf{u} \cdot \mathbf{u}' \rangle &= \frac{u^2}{r} \frac{\partial}{\partial r}(r^2 f) - 2u^2 + 2u^2 \\ &= \frac{u^2}{r} \frac{\partial}{\partial r}(r^2 f) - \frac{u^2}{r} \frac{\partial}{\partial r}(r^2) + 2u^2 \\ &= -\frac{1}{2r} \frac{\partial}{\partial r}(2u^2(1-f)r^2) + 2u^2 \end{aligned} \tag{S5}$$

The correlation tensor Q_{xx} and the second order structure function $\langle \delta u_L^2 \rangle$ are related by [7, p. 582, changing his structure function notation to that used elsewhere in this paper]

$$Q_{xx}(r\hat{\mathbf{e}}_x) = u^2 f(r) = u^2 - \frac{1}{2} \langle \delta u_L^2 \rangle \tag{S6}$$

We can re-arrange this equation to obtain the structure function:

$$\langle \delta u_L^2 \rangle = 2u^2(1-f) \tag{S7}$$

Substituting the right hand side into equation (S5) above we obtain

$$\langle \mathbf{u} \cdot \mathbf{u}' \rangle = -\frac{1}{2r} \frac{\partial}{\partial r}(r^2 \langle \delta u_L^2 \rangle) + 2u^2$$

$2u^2$ can be replaced with $\langle \mathbf{u} \cdot \mathbf{u}' \rangle$ using equation (S4), so substituting this in and rearranging for $\langle \delta u_L^2 \rangle$ we can write the longitudinal 2nd order structure function $\langle \delta u_L^2 \rangle$ in terms of the autocorrelation function $\langle \mathbf{u} \cdot \mathbf{u}' \rangle$

$$\langle \delta u_L^2 \rangle = \frac{2}{r^2} \int r \Big(\langle \mathbf{u} \cdot \mathbf{u} \rangle - \langle \mathbf{u} \cdot \mathbf{u}' \rangle \Big) dr \tag{S8}$$

which can be calculated starting from the 1D energy spectrum $E_1(k)$, using equation (S2). This analytical result is an indefinite integral, valid for $r > 0$ only, with the constraint $\langle \delta u_L^2 \rangle = 0$ at $r = 0$. In practice it must usually be evaluated numerically for discrete values of r as the definite integral

$$\langle \delta u_L^2 \rangle(r) = \frac{2}{r^2} \int_0^r r' \Big(\langle \mathbf{u} \cdot \mathbf{u} \rangle - \langle \mathbf{u} \cdot \mathbf{u}' \rangle(r') \Big) dr' \tag{S9}$$

In the Jupiter case, we can evaluate equations (S2) and (S9) directly using the measured eddy kinetic energy spectrum, but it is also instructive to consider an idealised case where the measured spectra are approximated by a flat region at low wavenumber and a $-5/3$ power-law slope at high wavenumber:

$$E_1(n) = \begin{cases} E_0 & n < n_1 \\ E_0 \left(n_1/n\right)^{5/3} & n \geq n_1 \end{cases}$$

where $n = 2\pi a/r$ is the non-dimensional wavenumber. Davidson [7, p. 91] defines $k = \pi/r$ so we write E_1 in terms of k by combining these two to get $n = 2ak$:

$$E_1(k) = \begin{cases} 2aE_0 & k < k_1 \\ 2aE_0 \left(k_1/k\right)^{5/3} & k \geq k_1 \end{cases} \qquad k_1 = n_1/(2a) \tag{S10}$$

Equation (S10) was fit to datasets G14g and C11 using nonlinear least squares in log-log space, giving the parameters in Supplementary Table 2. Supplementary Figure 1 shows the fits. At $r = 0$ the integral in equation (S2) is straightforward and gives $\langle \mathbf{u} \cdot \mathbf{u} \rangle = 10aE_0k_1$ analytically. $\langle \mathbf{u} \cdot \mathbf{u}' \rangle$ must be found numerically as the integral $\int_{k_1}^{\infty} k^{-5/3} \cos(kr) dk$ doesn't have a straightforward analytical solution. Supplementary Figures 2 and 3 show the resulting autocorrelation function $\langle \mathbf{u} \cdot \mathbf{u}' \rangle$ and 2nd order longitudinal structure function $\langle \delta u_L^2 \rangle$ predicted from our measured spectra and the fitted spectra using equation (S10).

Supplementary Table 1: **Parameters fitting equation (S10) to the eddy kinetic energy spectra.** Note that only one of n_1, k_1, and r_1 is a free parameter. Errors are standard deviations in the fitted values. The last two columns are included for information.

Dataset	E_0 ($\mathrm{J\,kg^{-1}}$)	n_1	k_1 ($\mathrm{m^{-1}}$)	r_1 (km)	$\langle \mathbf{u} \cdot \mathbf{u} \rangle$ ($\mathrm{m^2\,s^{-2}}$)	$\lvert\mathbf{u}\rvert$ ($\mathrm{m\,s^{-1}}$)
G14g	3.4±0.1	62.37±0.08	(4.461±0.006)×10^{-7}	7043±9	1060±30	32.6±0.5
C11	2.9±0.1	47.09±0.09	(3.368±0.007)×10^{-7}	9330±20	680±20	26.1±0.5

The 2nd order structure function that emerges has the following properties:

- It is flat for medium-large separations (which we observe in the measured structure function) due to the flat part of the spectrum at $k < k_1$.
- For small separations the structure function begins close to $r^{2/3}$ but rapidly becomes shallower as it transitions to flat (which we also observe).
- The range of observed separations where pure $r^{2/3}$ is expected is very narrow (up to at most $r \approx 1000\,\mathrm{km}$).

If the flat part of the spectrum is removed and the calculation repeated with $E_1(k) = 2aE_0(k_1/k)^{5/3}$, then the structure function reverts to the $r^{2/3}$ form (Supplementary Fig. 3, dotted lines).

There are some quantitative differences between the expected (Supplementary Fig. 3) and the measured (Supplementary Fig. 2) structure functions:

- The measured structure function is about 50-60% of the expected magnitude.
- The value of r where the expected structure function flattens out is a factor ∼2–3 larger than measured.

However, there are several details about the comparison that mean one should not expect quantitative agreement:

- The definition of the measured energy spectrum will be slightly different (i.e. with a different normalisation factor, being defined in terms of spherical harmonics, and with different definitions of wavenumber) from the definition used in the integral transform between the the energy spectrum and the autocorrelation function used above [7, equation (8.37)].

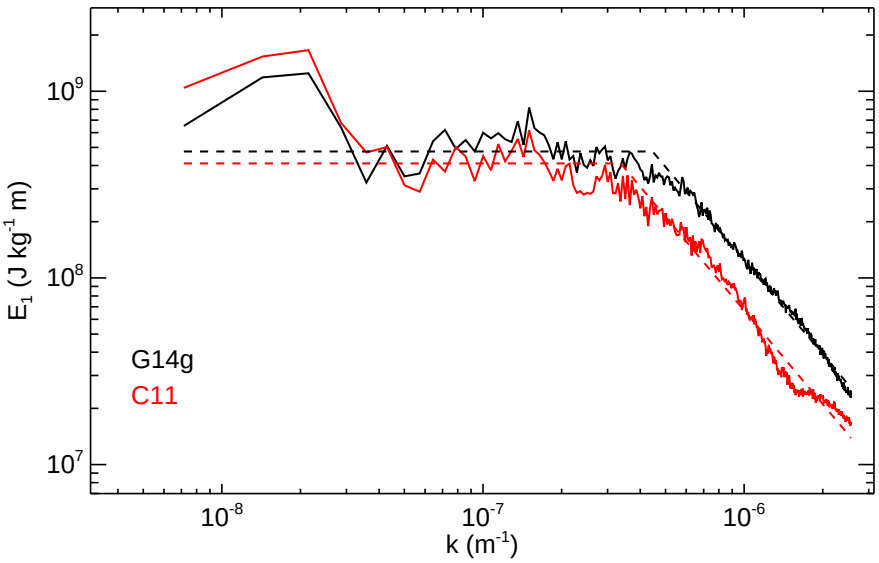

Supplementary Figure 1: **Measured Jovian eddy kinetic energy spectra $E_1(k)$ and fits using equation (S10).** Measured energy spectra from datasets G14g and C11 are shown in solid black and red respectively. Fits are shown as dashed lines.

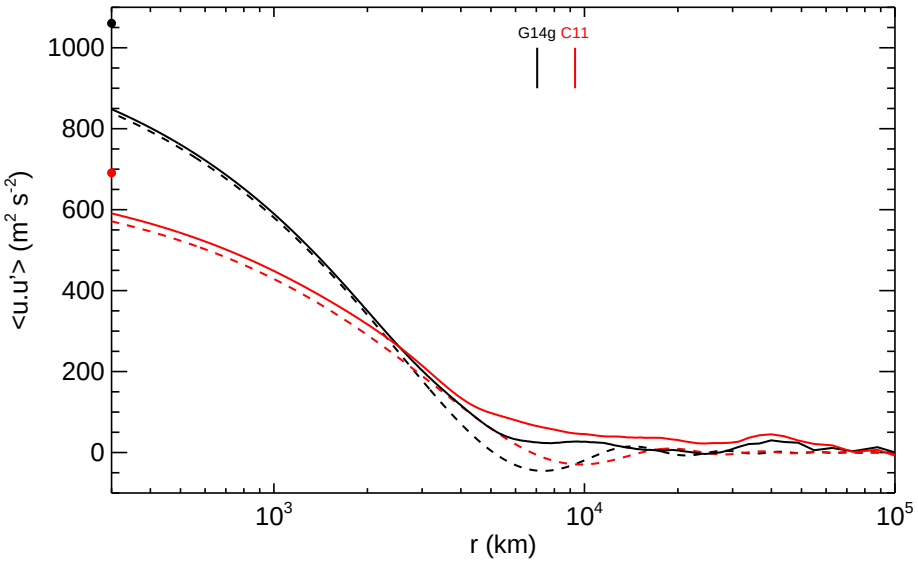

Supplementary Figure 2: **Autocorrelation function $\langle \mathbf{u} \cdot \mathbf{u}' \rangle$ derived from the kinetic energy spectra using equation (S2).** Lines and colours are as Supplementary Fig. 1. The vertical lines indicate r_1 for each dataset. The circles on the y-axis indicate the values that the black and red curves tend towards as $r \to 0$, i.e. $\langle \mathbf{u} \cdot \mathbf{u} \rangle = 10 a E_0 k_1$. Oscillations about zero in the fitted curves near k_1 are due to the Gibbs phenomenon, as dE_1/dk is discontinuous there.

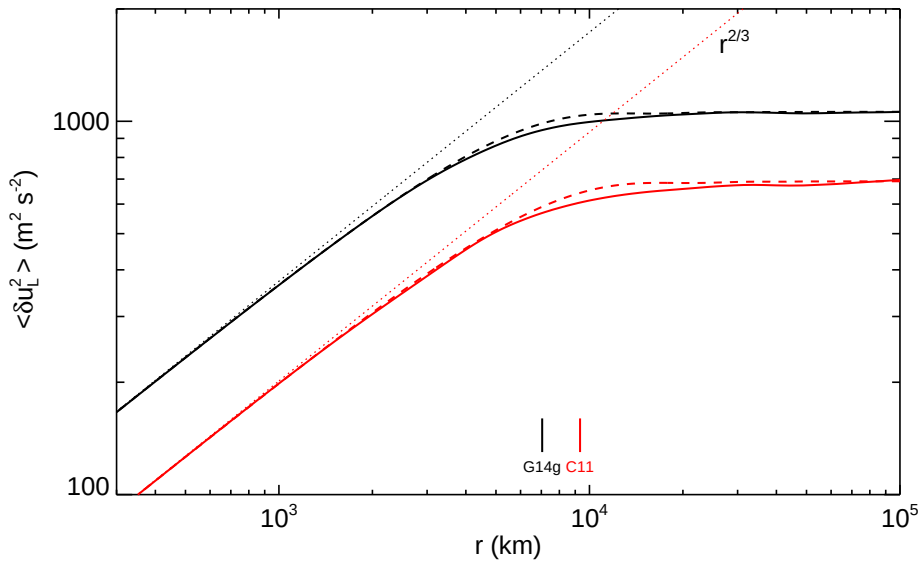

Supplementary Figure 3: **Expected 2nd order longitudinal structure functions using the measured kinetic energy spectra from Jupiter and equation (S9).** Lines and colours are as Supplementary Fig. 1. The dotted lines show the case $E_1(k) = 2aE_0(k_1/k)^{5/3}$, which results in pure $r^{2/3}$ scaling.

- There are differences in the data and data processing when computing the measured spectra (from gridded mosaics) and the structure functions (using individual velocity vectors, which have a larger variance than the gridded data, see Supplementary Fig. 5). See, for example, the blue line in Fig. 3a in the main text, which is the energy spectrum using just the individual images. The $n^{-5/3}$ range is somewhat smaller in that case.
- The calculation assumes both homogeneity and isotropy, neither of which we expect to be perfectly satisfied in Jupiter's atmosphere.
- The curvature of the planet's surface will have some effect on the measured structure function.

A note on isotropy This calculation assumes the flow is isotropic. It is useful to check that this is reasonable for the Jupiter data within the separation range of interest (i.e. up to the jet scale). One expects Jupiter's flow to be anisotropic at large scales due to its rapid rotation, but there is no a priori reason why it shouldn't be isotropic at small scales, at least horizontally. One can use a relationship between $\langle \delta u_L^2 \rangle$ and $\langle \delta u_T^2 \rangle$ to check whether the flow is isotropic [8, equation (53)]:

$$\langle \delta u_T^2 \rangle = \frac{d}{dr}\Big(r \langle \delta u_L^2 \rangle \Big) \tag{S11}$$

For the Jupiter structure functions this produces Supplementary Fig. 4. Equation (S11) is satisfied for $2500\,\mathrm{km} < r < 25\,000\,\mathrm{km}$, i.e. between the deformation scale and the jet scale. The flow becomes anisotropic for $r > 25\,000\,\mathrm{km}$, as expected.

At scales smaller than L_D the two curves diverge. However, at scales $r < L_D$ the separation vectors are primarily along the N-S and E-W directions, plus some vector pairs near the $45°$ angle near $r \approx L_D$ (Supplementary Fig. 6b). This is because the velocity vectors, while irregular, are nevertheless arranged on a pseudo-regular grid in longitude and latitude. Therefore the available data at small r, and hence the structure functions, do not sample the range of angles available, instead being biased towards the E-W and N-S directions. We don't have any information about other angles, so using the relationship between the second order structure functions at these scales to make a statement about isotropy is unreliable.

The 2D kinetic energy spectrum gives another estimate of how isotropic the flow is, as for isotropic flow the 2D spectrum should be independent of the zonal wavenumber m. This approach avoids the sampling problem the structure

functions have. The 2D kinetic energy spectra for datasets G14g and C11 are shown in Supplementary Fig. 13. These suggest the flow is reasonably isotropic at small scales, so we can conclude on this basis that the assumption of isotropy is reasonably well satisfied for the scales of interest.

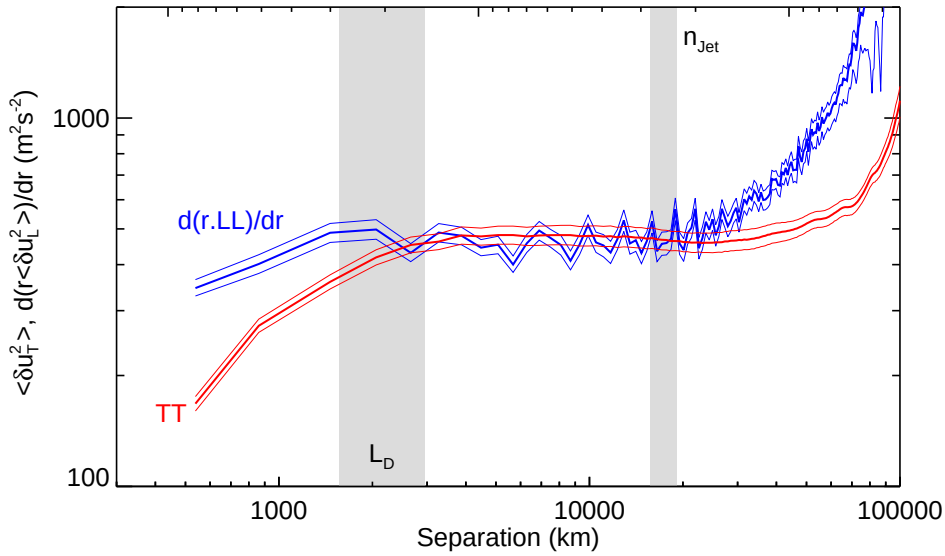

Supplementary Figure 4: **Isotropy relation between the 2nd order structure functions.** 2nd order transverse structure function (red) and derivative of the 2nd order longitudinal structure function (blue), using dataset G14s. The thick lines show the means and the thin lines their 95% confidence intervals. Light grey shading shows the jet scale and the typical deformation radius L_D between latitudes 20-40°.

3 Additional figures

Supplementary Figures 5-13 show

- 5: Zonal-time mean velocity and eddy velocity variability profiles for each dataset.
- 6: Number statistics for structure function vector pairs.
- 7: Estimated spread in the spectral fluxes and eddy-zonal conversion.
- 8: Estimated spread in the eddy kinetic energy spectra.
- 9: Zonal kinetic energy spectrum and estimated spread.
- 10: Enstrophy spectrum and estimated spread.
- 11: Compensated eddy kinetic energy spectra.
- 12: 2D kinetic energy and enstrophy spectra.
- 13: 3rd order structure functions for separations along E-W and N-S directions.

References

[1] Showman, A. P., Cho, J. Y.-K. & Menou, K. Atmospheric Circulation of Exoplanets. *arXiv:0911.3170* (2009).

[2] Sánchez-Lavega, A., Pérez-Hoyos, S. & Hueso, R. Clouds in planetary atmospheres: A useful application of the Clausius-Clapeyron equation. *Am. J. Phys.* **72**, 767–774 (2004).

[3] Irwin, P. *Giant Planets of our Solar System* (Springer/Praxis, 2009), 2nd edn.

[4] Weiss, J. *Planetary parameters*, In Bagenal, F., Dowling, T. E. & McKinnon, W. B. (eds.) *Jupiter: The Planet, Satellites and Magnetosphere*, chap. Appendix 2, 699–706 (Cambridge University Press, 2004).

[5] Read, P. L. *et al.* Mapping potential-vorticity dynamics on Jupiter. I: Zonal-mean circulation from Cassini and Voyager 1 data. *Q. J. R. Meteorol. Soc.* **132**, 1577–1603 (2006).

[6] Achterberg, R. K. & Ingersoll, A. P. A Normal-Mode Approach to Jovian Atmospheric Dynamics. *J. Atmos. Sci.* **46**, 2448–2462 (1989).

[7] Davidson, P. A. *Turbulence: An Introduction for Scientists and Engineers* (Oxford University Press, 2015), 2nd edn.

[8] Lindborg, E. Can the atmospheric kinetic energy spectrum be explained by two-dimensional turbulence? *J. Fluid Mech.* **388**, 259–288 (1999).

[9] Porco, C. C. *et al.* Cassini Imaging of Jupiter's Atmosphere, Satellites, and Rings. *Science* **299**, 1541–1547 (2003).

Supplementary Figure 5: **Zonal-time mean velocity and eddy velocity variability profiles for each dataset.** Variability is the standard deviation along each latitude circle. G14g is black (first three mosaics only used for time means), C11 is red, and G14s is blue. The dashed line in **a** is from Porco et al. [9, Fig. 1]. Note that in **b** and **d** the mosaiced dataset G14g (black) has noticeably lower variability than the sparse dataset G14s (blue).

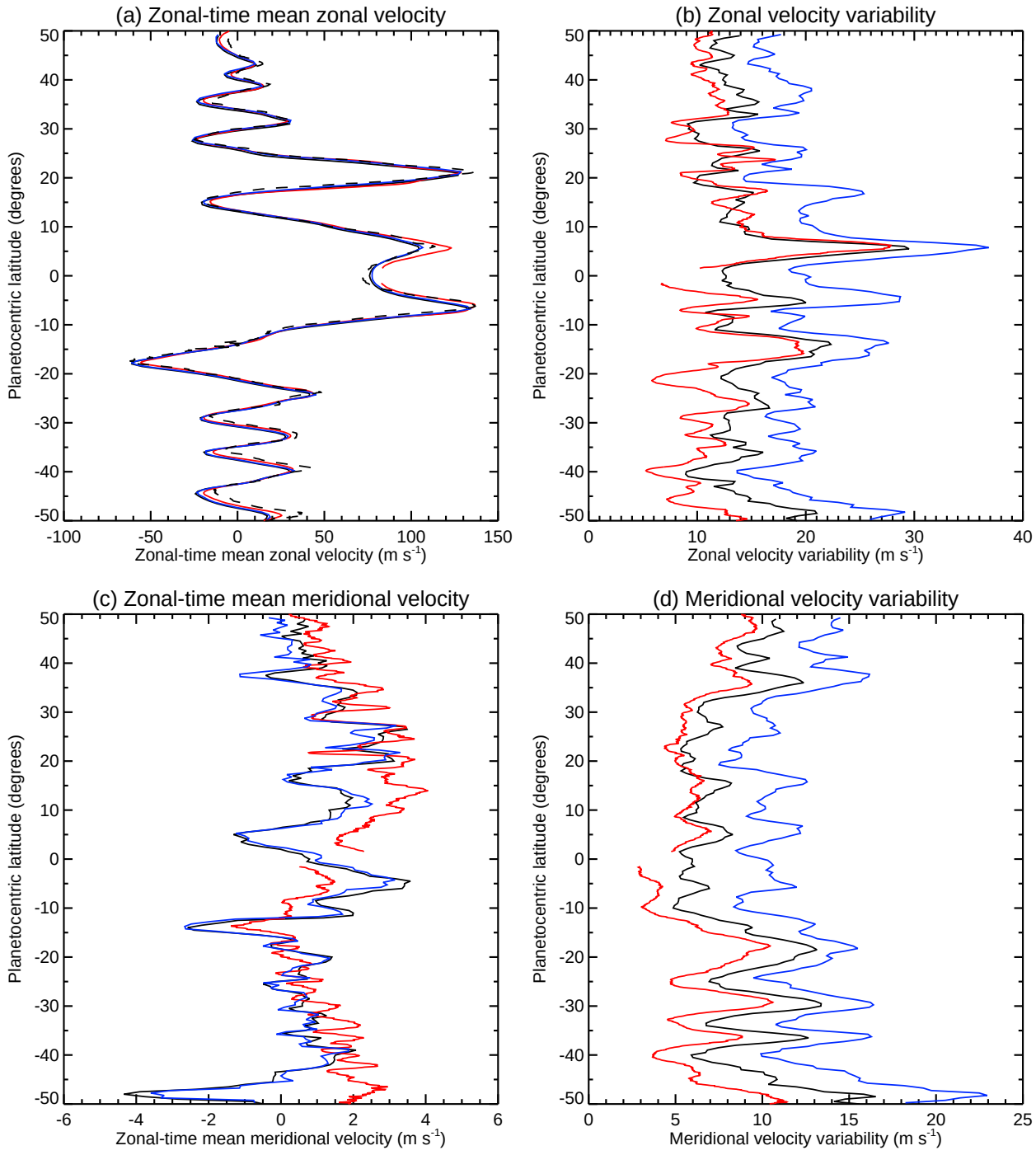

Supplementary Figure 6: **Number statistics for structure function vector pairs. a**, Distribution of the number of velocity vector pairs as a function of separation in dataset G14s. Each bin is $600\,\mathrm{km}$ wide and the number of points in each bin is indicated on the right. **b**, Distribution of the angle the vector separating each pair of velocity vectors makes with due North, as a function of separation (darker→more vector pairs). The distribution is skewed at large separation as vector pairs are taken between the corners of the image pair, and is skewed at small separation due to the quasi-regular gridded layout of the velocity vectors. The bearings are restricted to $0-90^\circ$ as the distinction between the start and end of each vector is arbitrary, and the system (NB: not the flow itself) is symmetric about the equator (so bearings 70° and 110° are equivalent, for example).

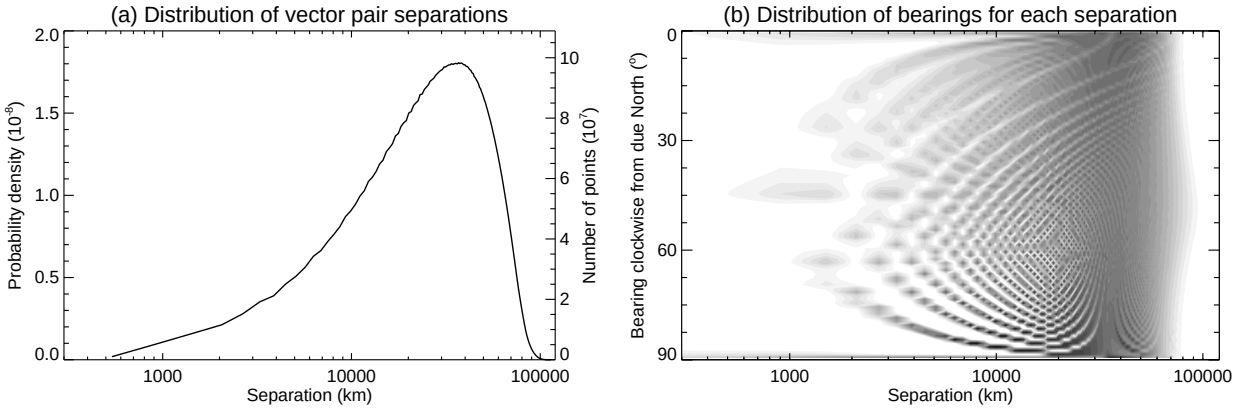

Supplementary Figure 7: **3rd order structure functions for separations along the East-West and North-South directions.** Black lines show structure functions averaged over all angles, as in Fig. 2a of the main manuscript. Red lines show structure functions for separations in the East-West direction only (where the separation vector falls within 0.5° of the East-West line), and blue lines show separations in the North-South direction only (equivalent 0.5° condition). Dots show negative values. Shaded areas are the same as Supplementary Fig. 4.

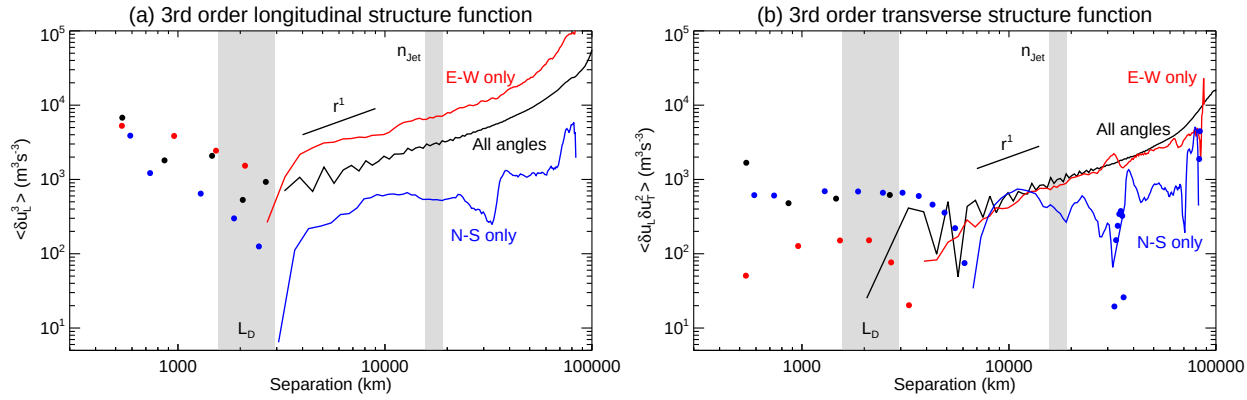

Supplementary Figure 8: **Estimated spread in the spectral fluxes and eddy-zonal conversion.** The coloured lines are the kinetic energy and enstrophy fluxes shown in Figs 3(c-f) of the main manuscript. Here each of those lines is shown separately, with an estimate of the spread of values over the dataset (either over the three days, in the case of G14g and C11, or over the individual image pairs, in the case of G14s). The spread at each wavelength (dark grey shaded area) is the standard deviation of the individual instances at that wavelength. The G14s plots are scaled in the same way as in the main manuscript.

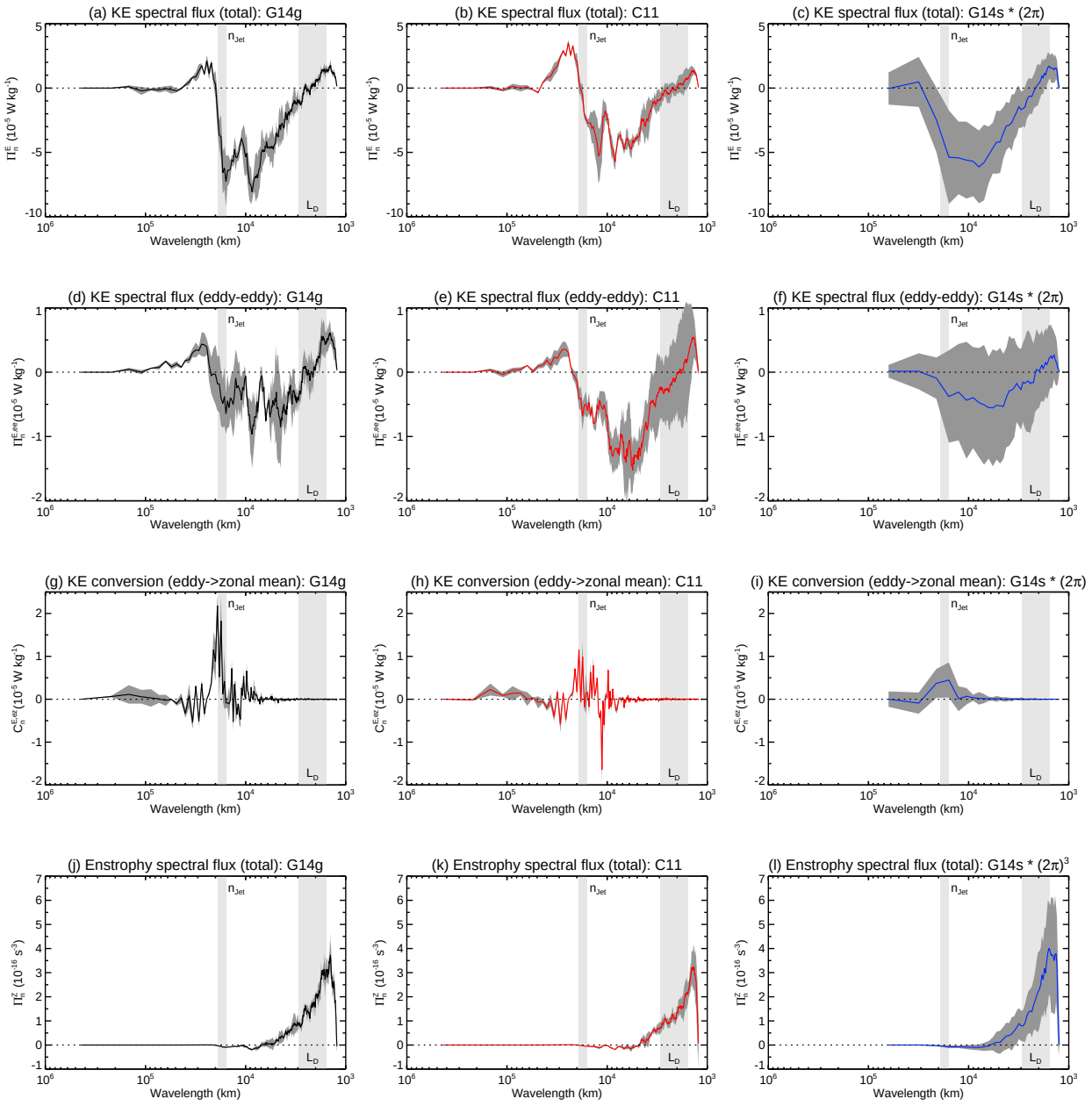

Supplementary Figure 9: **Estimated spread in the eddy kinetic energy spectra.** These show the spread of values for the lines in Figs 3(a-b) of the main manuscript. Lines and shading are the same as in Supplementary Fig. 8.

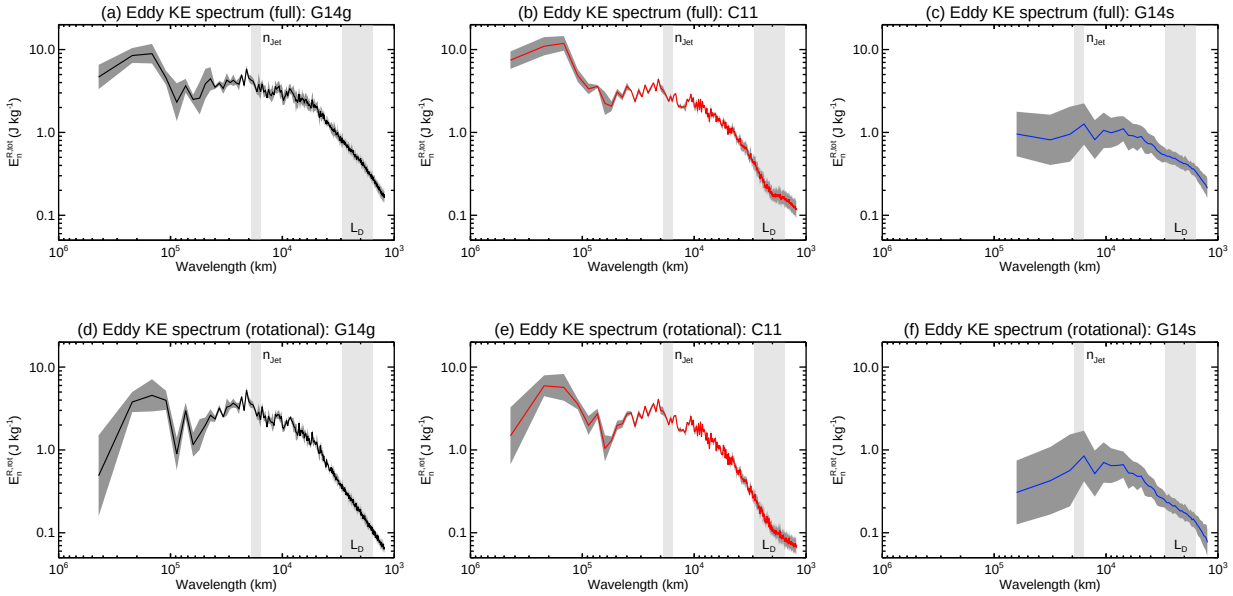

Supplementary Figure 10: **Zonal kinetic energy spectrum and estimated spread.** Lines and shading are the same as in Supplementary Fig. 8.

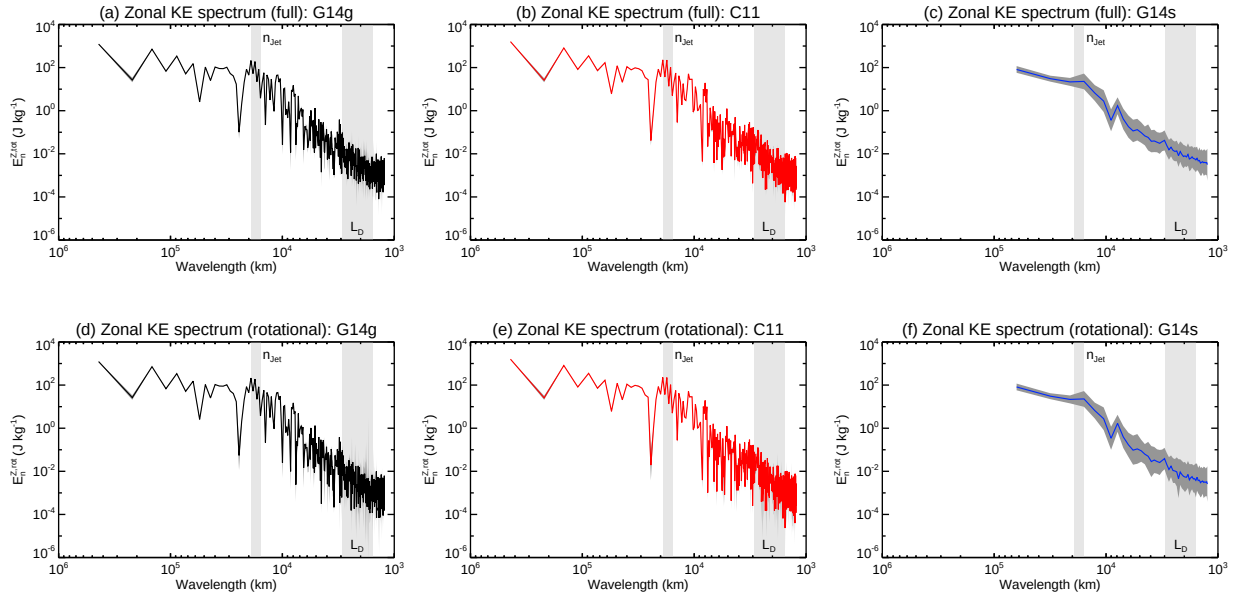

Supplementary Figure 11: **Enstrophy spectrum and estimated spread.** Lines and shading are the same as in Supplementary Fig. 8.

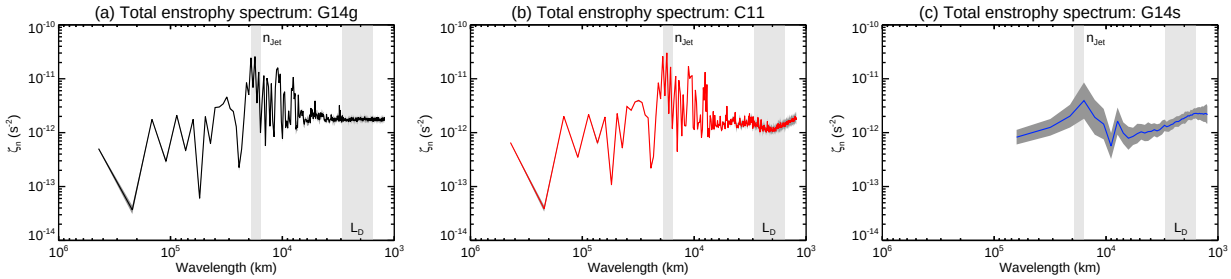

Supplementary Figure 12: **Compensated eddy kinetic energy spectra. a** and **b** are compensated by the fit lines plotted in Figs 3(a-b) in the main text, respectively. **c** and **d** are compensated by the wavenumber power that fits the spectrum at and just smaller than the jet scale. Lines and shaded regions are the same as Fig. 3 in the main text.

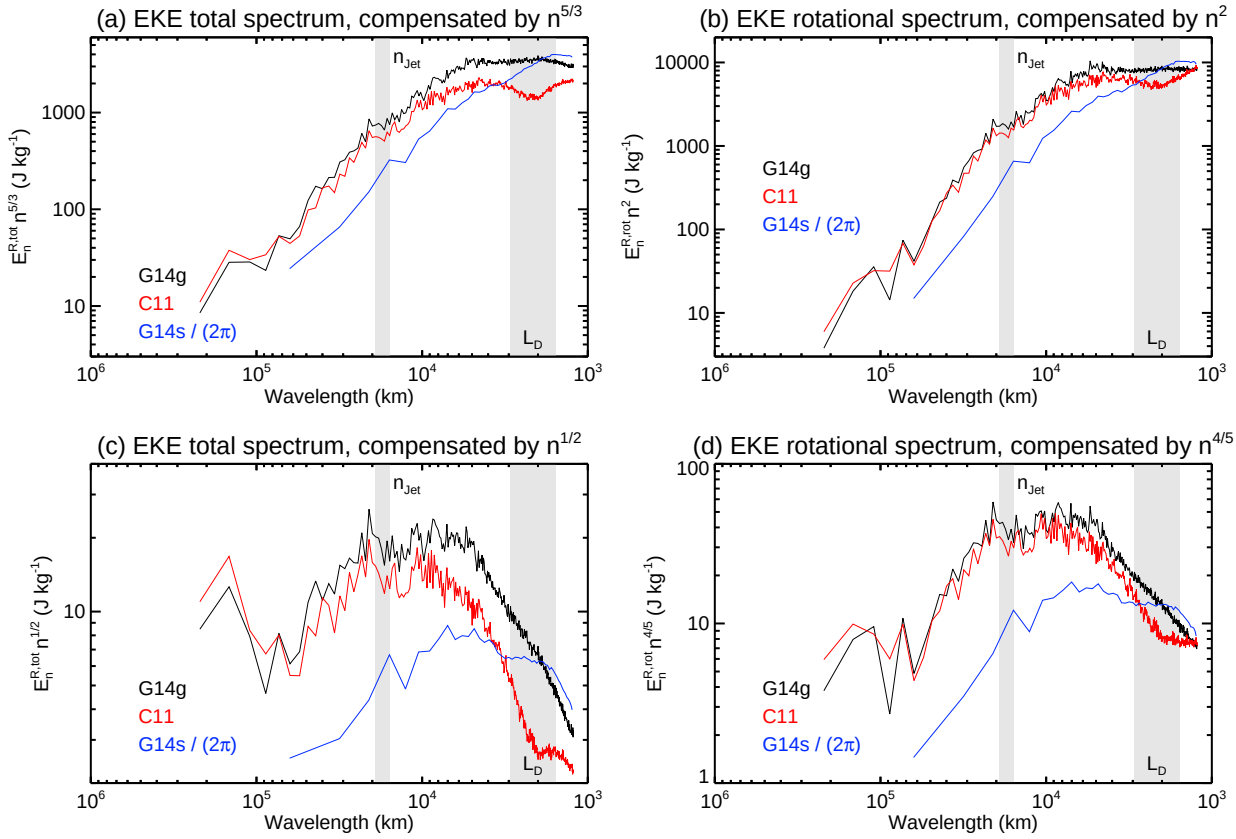

Supplementary Figure 13: **2D kinetic energy and enstrophy spectra.** Colours are shown on a log scale. Horizontal dashed lines bracket the range of deformation scales shown as grey bands in other figures, and horizontal dotted lines bracket the range of jet scales.